http://ansinet.com/itj

ITJ

ISSN 1812-5638

INFORMATION TECHNOLOGY JOURNAL

ANSInet
Asian Network for Scientific Information
308 Lasani Town, Sargodha Road, Faisalabad - Pakistan

Information Technology Journal 10 (12): 2406-2412, 2011
ISSN 1812-5638 / DOI: 10.3923/itj.2011.2406.2412

Prediction of Process Parameters on Stress and Strain Fields in Hot Rolling Process using Finite Element Method

[1]Licheng Yang, [2]Jinchen Ji, [1]Jinxiang Hu and [1]Liwei Ning
[1]Hunan Institute of Engineering, China
[2]University of Technology, Sydney, Australia

Abstract: To predict the distribution of stress and strain fields in hot rolling process, the computer models are built using rigid-plastic finite element method and are calculated using up-dated Lagrange method. The workpiece and the work-roll are defined as the deformation body and the rigid body with heat transfer, respectively. All kinds of heat boundary conditions, initial boundary and heat generation are introduced in the model. The analysis is capable of considering the effects of various parameters such as rolling speed, reduction ratio and tension rolling on effective strain, effective stress, contact normal stress and friction stress. In addition, the distributions of stress and strain and strain history are also calculated along contact arc length and thickness direction in the hot rolling process. To assess the reliability of the numerical analysis, a comparison is made between the prediction results and published literature and a reasonable agreement is obtained in this study.

Key words: Hot rolling, thermo-mechanical coupling, tension rolling, computer modeling

INTRODUCTION

Metal roll forming is widely used for manufacturing the semifinished, finished products and metallic equipment. The hot flat rolling is one of the most practical and popular forming processes. The essence of rolling process can be described that large plastic deformation occurs in the workpiece through multi-pass process under the application of friction force at the workpiece-rolls interface. The forming process involves in material, geometry and contact non-linearities, in addition, the interaction phenomena occur among the parameters of temperature, deformation, force and energy. Therefore, it is impossible to analytical solutions for all kinds of mechanical and deformation parameters in the hot rolling process. In the past decades, finite element method (Lee, 1998; Kim *et al*., 2005) finite difference method (Chung *et al*., 1993) boundary element method (Gonzalez and Abascal, 1998) and upper bound methods (Sheikh, 2009) have been carried out with considerable success in calculating the cold/hot rolling process. The simulation results mainly depend on the reasonable assumption, definition of thermal transfer boundary conditions and initial conditions.

Prediction of deformation and mechanical properties in hot rolling is of importance to field engineers in order to manufacture high quality and quantity products. There are many studies concentrating on evaluating the stress and strain fields in the rolling process. Hwang and Tzou (1996), Bayoumi (1997), Chang (1999) and Sun *et al*. (2010) studied all kinds of stress distributions, such as rolling pressure distribution, horizontal stresses, shear stresses, edge stress and thermal stress. Vallellano *et al*. (2008) predicted the contact stress distributions in the roll-wire contact zone, residual stresses and contact pressure using a 3D numerical analysis. The study of the effect of process parameters on stress and strain fields has been another research topic. The effect of various process parameters, including reduction ratio, rolling speed and initial temperature, on the detailed aspects of interfacial thermo-mechanical behavior of the roll and strip, such as friction coefficient and ratio of pressure to flow stress, was investigated by Sun (2005). Arif *et al*. (2004) calculated pressure distribution and friction stress and studied Von Mises stress inside the roll at different radius. Based on software FORGE3, the contact pressure distribution, equivalent strain history and distribution were simulated by Duan and Sheppard (2002). Serajzadeh *et al*. (2002) used rigid-viscoplastic FEM to predict the strain distributions within the rolled metal at different positions in the deformation zone and the effect of various process parameters, such as initial strip temperature, rolling speed, lubrication on the strain in the hot rolling process.

In the present study, the finite element modeling of heat transfer and deformation is considered in the hot

Corresponding Author: Licheng Yang, Hunan Institute of Engineering, China

rolling process of a strip. The various thermal transfer phenomena, such as radiation and convection between the workpiece and the surrounding environment (air cooling), contact thermal conduction at the workpiece-rolls interface, heat generation due to plastic deformation and friction work (inner heat resource), forced heat convective of water (water cooling) and inner heat conduction, are introduced in the model. The effect of process parameters, including rolling speed, reduction ratio, initial strip thickness, friction factor and tension rolling, on effective strain, effective stress, contact normal stress and friction stress are inverstigated in this study. The distributions of stress, strain and strain rate, strain history and normal pressure are also calculated in the hot rolling process.

MODELING

Thermo-mechanical coupled model: In the hot rolling process, the temperature distribution of the strip and the work-rolls can be calculated using the governing partial differential can be shown as follows:

$$\frac{\partial}{\partial x_i}\left(\lambda_{ij}\frac{\partial T}{\partial x_j}\right)+\dot{q}-\rho c\frac{\partial T}{\partial t}=0 \quad (1)$$

where, $\dot{q}$, ρ, c, t and λ_{ij} are heat generation rate per unit volume, density, specific heat, time and thermal conductivity coefficient, respectively.

In Table 1, All kinds of conditions are used to solve Eq. 1 which involves in heat convection and radiation (air cooling), forced convective boundary condition of water (water cooling), contact heat conduction at the workpiece-roll interface, inner conduction due to the temperature gradient between the core and the surface in the strip, heat generation due to plastic deformation and friction work, adiabatic boundary in symmetric center of the strip and initial conditions. The physical meaning of the parameters in these equations are defined as follows: q_{con} is heat flux due to contact conduction, h_{con} is heat conduction coefficient, T_s is the strip temperature, T_r is the work-roll temperature, q_a is thermal losses due to heat convection and radiation, h_c is heat transfer coefficient, T_a is the room temperature, σ_{st} is Stenfan-Boltzmann constant, ε_r is the surface emissivity, q_w is heat losses due to water cooling, h_w is the forced convective coefficient, T_w is water temperature, q'_{con} is heat transfer from the core to surface due to the temperature difference, h'_{con} is heat transfer coefficient of the strip, T_{surf} is the surface temperature, T_{core} is the core temperature, q is$_f$ heat generation due to friction work, τ_f is the friction shear stress, A_c is the contact area, v_r is the relative slipping velocity along the arc of contact, δt is time increment step, $\dot{q}_{def}$ is heat generation rate due to plastic deformation, η is the efficiency of conversion of deformation energy to heat, $\bar{\sigma}$ is effective flow stress, $\dot{\bar{\varepsilon}}$ is the equivalent strain rate, T_1 is initial strip temperature and T_2 is initial roll temperature.

Table 1: Boundary conditions of heat transfer models

Conditions	Equations
Contact conduction	$q_{con}=h_{con}(T_s-T)$
Air cooling	$q_a=h_c(T_s-T_a)+\sigma_{st}\varepsilon_r(T_s^4-T_a^4)$
Water cooling	$q_w=h_w(T_s-T_w)$
Iuner conduction	$q'_{con}=h'_{con}(T_{core}-T_{surf})$
Heat generation	$q_f=\tau_f A_c v_r \delta t$
	$\dot{q}_{def}=\eta\bar{\sigma}\dot{\bar{\varepsilon}}$
Adiabatic boundary	$\frac{\partial T(y,t)}{\partial y}=0 \quad (y=0)$
Initial conditions	$T_s(t)=T_1 \quad (t=0)$
	$T_r(t)=T_2 \quad (t=0)$

Models of stress and strain: The linear strain β $(T-T_0)$ occurs when the workpiece temperature changes where β is linear thermal dilation coefficient of the material, T is the present temperature of the elastic material and T_0 is the initial workpiece temperature. The corresponding stress occurs due to the constraint of the roll in the rolling process. Temperature affects structural stress and deformation which produces thermal stress and thermal strain. Moreover, the mechanical properties, such as elastic module, Poisson ratio, yield stress and thermal dilation coefficient, usually vary with the temperature which also affects structural stress. The balance relation of stress on the element and equivalent external force P on the node can be described as:

$$\int_V B^T\sigma dV=P \quad (2)$$

where, V is spatial domain, B^T is transfer matrix between the total stress ε of the element and the nodal displacement u:

$$\varepsilon=Bu \quad (3)$$

The total strain usually consists of three kinds of strain:

$$\varepsilon=\varepsilon^e+\varepsilon^p+\varepsilon^T \quad (4)$$

where, ε^e, ε^p and ε^T show elastic strain, plastic strain and thermal strain due to temperature, respectively.

Analysis of elastic strain. The elastic strain ε^e should satisfy Hooke law:

$$\sigma=D\varepsilon \quad (5)$$

where, D is elastic coefficient matrix. It is assumed that the plastic strain of thermal elastic-plastic material follows J_2 flow theory and Eq. 5 can be given by the incremental format of plasticity:

$$\Delta\sigma = D_T\Delta\varepsilon\text{-}h\Delta T \tag{6}$$

where, D_T is elastic-plastic coefficient matrix and depends on temperature which involves in the contribution of elastic deformation and plastic deformation. h shows the tensor of the contribution of thermal strain on stress. From the preceding Eq. 2, 3 and 6, the equation can be obtained:

$$\int_V B^T D_T B\Delta u dV = \Delta P + \int_V B^T h\Delta T dV \tag{7}$$

The term of left side in Eq. 7 shows the effect of tangent stiffness at the present temperature and the last term of right side denotes equivalent thermal load due to thermal strain which embodies the effect of the temperature in the analysis of thermal stress.

Thermal elastic-plastic analysis. The thermal elastic-plastic behavior shows the physical properties, such as elastic module, Poisson ratio, yield stress and work hardening curve, vary with temperature. Mises yield criterion shows material becomes plastic state when stress intensity equals yield limit when material was in uniaxial tension:

$$F = \sqrt{\frac{3}{2}S_{ij}S_{ij}} - \sigma_y\left(\varepsilon_{eq}^p, T\right) = 0 \tag{8}$$

where, S_{ij} is stress deviator, σ_y is yield stress and the function of equivalent plastic strain and temperature. The following equation can be obtained for the continuous hardening:

$$\frac{\partial F}{\partial \sigma_{ij}} - \frac{\partial \sigma_y}{\partial \varepsilon_{eq}^p}\dot{\varepsilon}_{eq}^p - \frac{\partial \sigma_y}{\partial T}\dot{T} = 0 \tag{9}$$

Equivalent plastic strain rate is given by:

$$\frac{\partial \varepsilon_{eq}^p}{\partial t} = \sqrt{\frac{2}{3}\dot{\varepsilon}_{eq}^p\dot{\varepsilon}_{eq}^p} \tag{10}$$

The corresponding equivalent stress (the effective value of conversion of multiaxial stress into uniaxial stress) is written as:

$$\sigma_{eq} = \sqrt{\frac{3}{2}S_{ij}S_{ij}} \tag{11}$$

According to the association flow rules of plastic strain increment based on yield surface normal and proportionality factor λ, the corresponding equivalent plastic strain rate is shown in:

$$\dot{\varepsilon}_{eq}^p = \lambda\frac{\partial F}{\partial \sigma_{ij}} = \lambda\frac{3S_{ij}}{2\sigma_{eq}} \tag{12}$$

The total strain rate involves in three kinds of strain rate,

$$\dot{\varepsilon}_{ij} = \dot{\varepsilon}_{ij}^e + \dot{\varepsilon}_{ij}^p + \dot{\varepsilon}_{ij}^T \tag{13}$$

where, $\dot{\varepsilon}_{ij}$, $\dot{\varepsilon}_{ij}^e$, $\dot{\varepsilon}_{ij}^p$ and $\dot{\varepsilon}_{ij}^T$ show the total strain rate, elastic strain rate, plastic strain rate and thermal strain rate, respectively. Similarly, the stress rate can be written as:

$$\dot{\sigma}_{ij} = D_{ijkl}(T)\dot{\varepsilon}_{kl}^e + C_{ij}\dot{T} \tag{14}$$

where, D_{ijkl} is elastic coefficient matrix. The coefficient matrix C_{ij} is given by:

$$C_{ij} = \frac{\partial D_{ijkl}(T)}{\partial T}\varepsilon_{kl}^e \tag{15}$$

According to Eq. 14 and 15, the constitutive relation of thermal elastic-plastic material can be obtained:

$$\dot{\sigma}_{ij} = D_{ijkl}\left(\dot{\varepsilon}_{kl} - \dot{\varepsilon}_{kl}^T - \lambda\frac{3S_{kl}}{2\sigma_{eq}}\right) + C_{ij}\dot{T} \tag{16}$$

Material properties: The material of the strip is a typical carbon steel and its chemical composition is defined as follows: 0.14% C, 0.27% Si, 0.35% Mn, 0.032% P, 0.024% S, 0.21% Ni, 0.18% Cr and 0.23% Cu. It obeys Von Mises yield criterion and the flow rule (Prandtl-Reuss equation). Uniform temperature distribution is assumed throughout the original strip. In the present study, the density of the strip is 7850 kg m^{-1} and the Poisson's ratio is 0.3. Other thermo-physical parameters of the strip, such as elastic module E, heat dilatation coefficient β, heat conduction rate λ and specific heat c, are all the function of temperature. The fiction model at rolls-workpiece interface is assumed to be non-linear shear friction model with constant friction factor. To save computing time, only half of the strip thickness is simulated in the model because of symmetry. Thermo-mechanical coupled FEM and isoparametric technology are used to build FEM model of hot-strip rolling and the coupled equation is solved using updated Lagrange method. The models of the workpiece and work-roll are shown in Fig. 1.

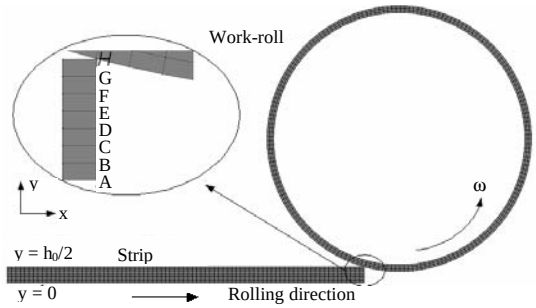

Fig. 1: Models of the strip and work-role and selected positions

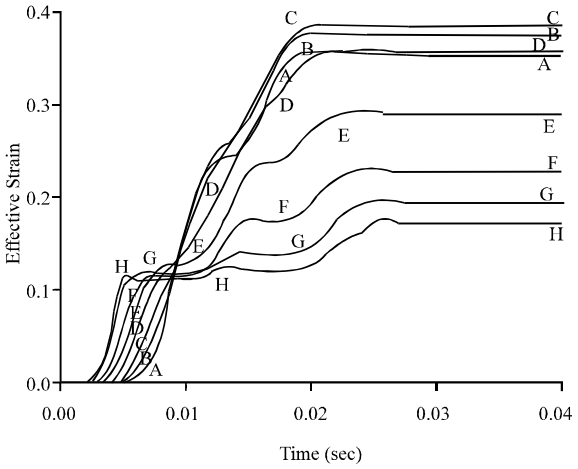

Fig. 2: Effective strains histroy in the different positions

RESULTS AND DISCUSSION

Effective strain history: Figure 2 shows effective strain varies with rolling time for different nodes along thickness direction. It can be seen that effective strain in the deformation zone vary significantly with time. The minimum effective strain is applied on the strip surface and the maximum effective strain occurs between the core position and the surface position which is agreement with the results of Riahifar and Serajzadeh (2007). It can be explained that the minimum temperature occurs on the surface due to the contact heat conduction at the workpiece-roll interface, heat convection and radiation between the workpiece and the surrounding environment. Because rolling process involves in biting, deforming and uninstall stages, all curves of effective strain always increases from zero gradually. For example, the effective strain of the core equals to 0.389 which shows strip rolling belongs to large plastic deformation.

Strain rate: In the deformation zone, Fig. 3 shows strain rate distribution on the cross section and it varies with different rolling speeds. It is observed that the maximum strain rate is applied in the entry of the deformation zone under the work-roll which keeps the same with the results of Shahani *et al.* (2009). It can be explained that the deformation in this position occurs suddenly. For two rotating speeds 5 and 10 rpm, it can be seen that strain rate 10.65 (1 sec^{-1}) happens in the entry of the deformation zone for rotating speeds 10 rpm. The higher rolling speed causes the higher speed of deformation and the strip and the work-roll to be less time in contact and the corresponding strain rate also increases.

Contact normal stress and friction stress: Figure 4 shows the distribution curves of friction stress along rolling direction and contact normal stress along the strip

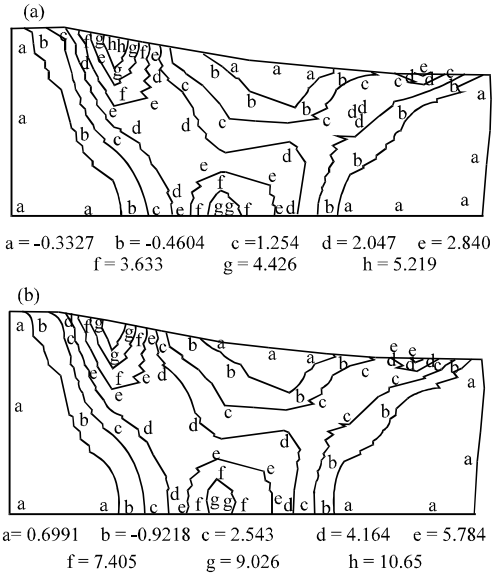

Fig. 3(a-b): Distribution of effective strain rate of the strip in the deformation zone for T_0 = 950, m = 0.15 and h_0 = 15mm, (a) n = 5 rpm, (b) n = 10 rpm

thickness direction on the contact arc. In Fig. 4a, the contact arc length increases from 24 to 34 mm when the roll radius increases from 160 to 360 mm and the contact normal stress rises from 606 to 658.46 MPa. It can be explained that the unit pressure will increase with the increasing roll radius which causes the corresponding contact normal stress rise. The distribution curves of friction stress for different roll radii are indicated in Fig. 4b. The friction stress is positive in backward slip zone where the strip entry velocity is less than the horizontal component of the roll linear velocity whereas, the friction stress is negative in forward slip zone where

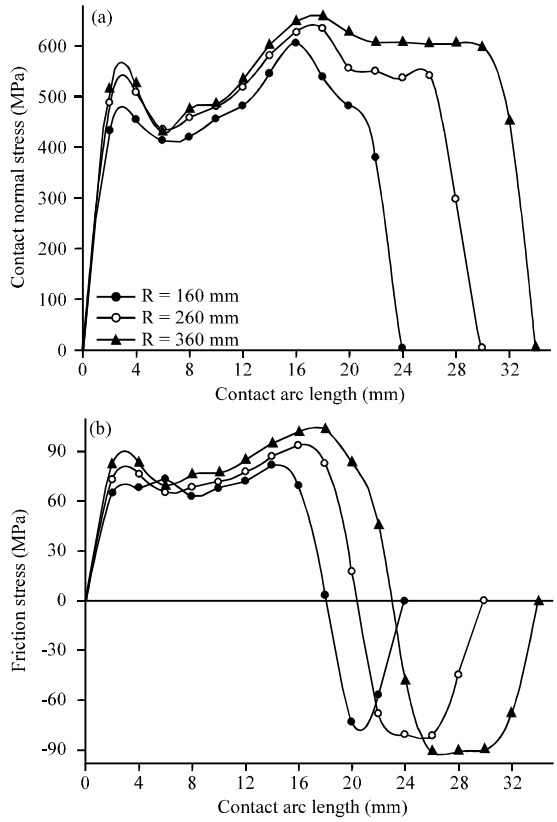

Fig. 4(a-b): The effect of roll radius on friction stress and contact normal stress for T_0 = 950°C, h_0 = 15 mm, r = 25%, m = 0.15 and n = 5 rpm

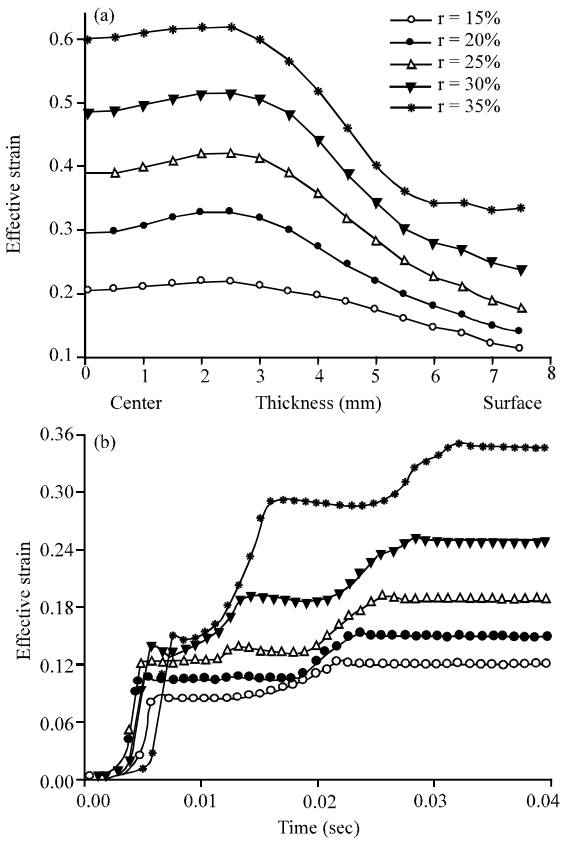

Fig. 5(a-b): The effect of reduction ratio on effective strain distribution for T_0 = 950°C, h_0 = 15 mm, r = 25%, m = 0.15 and n = 5 rpm

the exit velocity is more than the linear velocity of the roll. The division point of the positive and negative friction stress is just the position of neutral plate where friction stress equals to zero. The neutral plate is away from the entry position gradually with the increasing roll radius and which results in the positive friction zone increase. The maximum positive friction stress rises from 81.92 to 103.52 MPa and the minimum negative friction stress rises from 72.37 to 90.77 MPa when the roll radius increases by 200 mm. Moreover, the positive friction stress and its distribution zone are more than the negative friction stress and the corresponding distribution zone, respectively and this indicates friction force is the reason of metal rolling process.

Effect of reduction ratio on effective strain: Figure 5a shows the effect of reduction ratio on effective strain distribution through thickness direction at the exit of the deformation zone. It is observed that the amount of reduction ratio has a major influence on the effective strain distribution and magnitude. The effective strain of any points in the strip rises with the increasing reduction ratio. It can be easily explained that the displacement and deformation rises with the improvement of reduction ratio. For example, when reduction ratio increases from 15 to 35%, the maximum strain increases by 0.22 and the minimum strain increases by 0.40. In addition, the strain difference between the maximum strain and the minimum strain increases from 0.1078 to 0.2896 when reduction ratio increases by 20%. For different reduction ratios, it can be seen from Fig. 5b that the effective strain on the surface varies significantly with rolling time. The effective strain increases rapidly when the workpiece feeds into the roll gap and it keeps invariable after the completion of rolling process. The more reduction ratio results in longer contact length and higher effective strain on the surface. For example, when the reduction ratio rises from 15 to 35% with the incremental difference 5%, the strain increases by 0.0299, 0.0396, 0.0607 and 0.1005, respectively.

Effect of tension rolling on effective strain and contact normal stress: Tension occurs due to non-compatibility velocities or metal flow difference among tandem mills which has a major effect on the stability of rolling

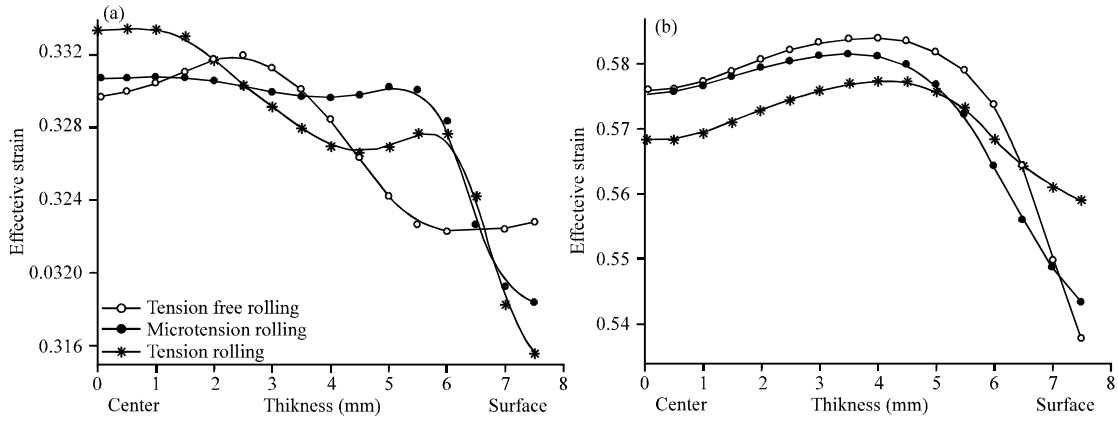

Fig. 6(a-b): The effect of tension rolling on effective strain; (a) the ith stand and (b) the (i = l)th stand

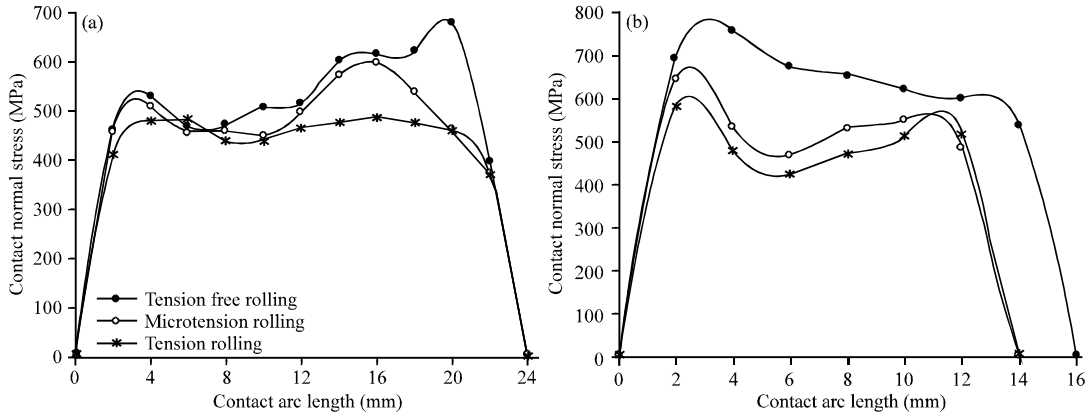

Fig. 7(a-b): The effect of tension rolling on contact normal stress; (a) the ith stand and (b) the (i + 1)th stand

process. The following conditions may cause the tension rolling. (1) If the exit velocity of the ith stand mill is reduced, or the forward slip quantity decreases due to the drop of the ith roll speed; (2) Tension rolling occurs because of the change of other process parameters, for example, reduction ratio; (3) If the entry velocity of (i + 1)th stand mill increases because of the increase of the (i+1)th roll speed or the decline of the backward slip magnitude which causes the tension produce. Figure 6 shows the effect of tension rolling on effective strain through the thickness direction. As shown in Fig. 6a, when the workpiece is in tension free rolling statue, the maximum effective strain occurs between the strip core and the strip surface and the minimum effective strain happens on the surface for the *i*th stand. For microtension rolling or tension rolling, the maximum effective strain gradually expands to the strip core. Moreover, the strain difference increases significantly, for example, the strain differences equals to 0.010, 0.012 and 0.018, respectively, for tension free rolling, microtension rolling and tension rolling. It can be seen from Fig. 6b that the effective strain distribution of (i+1)th stand mill is the just opposite of the ith stand mill. The maximum effective strain on the strip surface and the minimum effective strain in the strip core occur for tension rolling. In three rolling conditions, the maximum effective strain all occurs between the surface and the core. For tension free rolling, microtension rolling and tension rolling, the strain differences equals to 0.046, 0.038 and 0.0183, respectively.

Figure 7 shows that the effect of tension rolling on contact normal stress along contact arc length. For the ith stand, when the workpiece is in tension free rolling state, the maximum contact normal stress is closer to the exit of the ith stand. When the workpiece is in tension rolling state, the backward slip zone decreases and the corresponding contact normal stress decreases significantly and its distribution is very balance along the contact arc direction. For tension free rolling,

microtension rolling and tension rolling, the maximum contact normal stresses are 676.45, 599.86 and 488.02 MPa, respectively. In the (i+1)th stand, as shown in Fig. 7b, the maximum stress occurs at the entry of the workpiece for three rolling conditions. The minimum contact normal stress still occurs for tension rolling condition. The contact arc length of the tension free rolling is more than those of microtension rolling and tension rolling condition. For three rolling conditions, the maximum contact normal stresses are 754.73, 646.36 and 580.61 MPa, respectively.

CONCLUSIONS

To predict stress and strain fields in hot rolling of the strip, the models have been developed by using thermo-mechanical coupling finite element method. The simulation results provide reasonable agreement with the reported results available in the literature. The results can be shown as follows:

- The maximum strain rate is applied in the entry of the deformation zone under the work-roll. The contact normal stress and friction stress at the workpiece-roll interface increases with roll radius. The effective strain of any points in the strip rises with the increasing reduction ratio
- Tension rolling can improve the stability of rolling process which makes the effective strain difference smaller and causes normal stress decrease and gentler distribution along contact arc length

ACKNOWLEDGMENTS

The work is supported by National Natural Science Foundation of China and Baosteel Group (51004047), Scientific Research Fund of Hunan Provincial Education Department (10B020), Natural Science Foundation of Hunan (09jj4024).

REFERENCES

Arif, A.F.M., O. Khan and A.K. Sheikh, 2004. Roll deformation and stress distribution under thermo-mechanical loading in cold rolling. J. Mater. Process. Technol., 147: 255-267.

Bayoumi, L.S., 1997. Edge stresses in wide strip hot rolling. Int. J. Mech. Sci., 39: 397-408.

Chang, D.F., 1999. Thermal stresses in work rolls during the rolling of metal strip. J. Mater. Process. Technol., 94: 45-51.

Chung, S.G., K. Kuwahara and O. Richmond, 1993. Streamline-coordinate finite-difference method for hot metal deformations. J. Comput. Phys., 108: 1-7.

Duan, X. and T. Sheppard, 2002. Three dimensional thermal mechanical coupled simulation during hot rolling of Aluminium alloy 3003. Int. J. Mech. Sci., 44: 2155-2172.

Gonzalez, J. and R. Abascal, 1998. Using the boundary element method to solve rolling contact problems. Eng. Anal. Boundary Ele., 21: 385-392.

Hwang, Y.M. and G.Y. Tzou, 1996. Stress analysis of asymmetrical cold rolling of clad sheet using the slab method. J. Mater. Eng. Perform., 5: 621-631.

Kim, S.Y., H.W. Lee, J.H. Min, Y.T. Im, 2005. Steady state finite element simulation of bar rolling processes based on rigid-viscoplastic approach. Int. J. Num. Methods Eng., 63: 1583-1603.

Lee, J.D., 1998. A large-strain elastic-plastic finite element analysis of rolling process. Comput. Methods Applied Mech. Eng., 161: 315-347.

Riahifar, R. and S. Serajzadeh, 2007. Three-dimensional model for hot rolling of aluminum alloys. Mater. Des., 28: 2366-2372.

Serajzadeh, S., A.K. Taheri, M. Nejati, J. Izadi and M. Fattahi, 2002. An investigation on strain inhomogeneity in hot strip rolling process. J. Mater. Process. Technol., 128: 88-99.

Shahani, A.R., S. Setayeshi, S.A. Nodamaie, M.A. Asadi and S. Rezaiec, 2009. Prediction of influence parameters on the hot rolling process using finite element method and neural network. J. Mater. Process. Technol., 209: 1920-1935.

Sheikh, H., 2009. Thermal analysis of hot strip rolling using finite element and upper bound methods. Applied Math. Mod., 33: 2187-2195.

Sun, C.G., 2005. Investigation of interfacial behaviors between the strip and roll in hot strip rolling by finite element method. Tribol. Int., 38: 413-422.

Sun, J.L., Y. Peng, H.M. Liu and G.B. Jiang, 2010. Vibration of moving strip with distributed stress in rolling process. J. Iron Steel Res. Int., 17: 24-30.

Vallellano, C., P.A. Cabanillas, F.J. Garcia-Lomas, 2008. Analysis of deformations and stresses in flat rolling of wire. J. Mater. Process. Technol., 195: 63-71.